Frequency-Mixing Intelligent Reflecting Surfaces for Nonlinear Wireless Propagation

Yuan, Jide; De Carvalho, Elisabeth; Williams, Robin Jess; Bjornson, Emil; Popovski, Petar

Published in:
I E E E Wireless Communications Letters

DOI (link to publication from Publisher):
10.1109/LWC.2021.3077085

Publication date:
2021

Document Version
Accepted author manuscript, peer reviewed version

Frequency-Mixing Intelligent Reflecting Surfaces for Nonlinear Wireless Propagation

Jide Yuan, *Member, IEEE*, Elisabeth De Carvalho, *Senior Member, IEEE*, Robin Jess Williams, *Member, IEEE*, Emil Björnson, *Senior Member, IEEE*, and Petar Popovski, *Fellow, IEEE*

***Abstract*—We introduce the concept of frequency-mixing intelligent reflecting surface (FMx-IRS), where the elements of the surface continuously change the phases of the incident signals. In this way, the FMx-IRS acts as a frequency mixer and makes the propagation environment nonlinear, thereby introducing new frequencies. We study the basic features of the proposed concept and demonstrate its advantages that stem from the novel type of control over the wireless propagation. The channel decoupling feature and the correlation between reflected channels are elaborated for the architecture, and are validated by the simulations.**

***Index Terms*—Channel estimation, intelligent reflecting surface, nonlinear wireless propagation**

I. Introduction

An intelligent reflecting surface (IRS) consists of a large number of reflecting elements with tunable properties, which potentially can be used to unleash new operation modes and applications in wireless communications [1]. In a typical setting, the IRS can affect some of the dominant propagation paths between a user and a base station (BS). The objective is to align the signal phase of each path by choosing the phases of the reflecting elements, maximizing the signal-to-noise ratio (SNR) of the received signal. This type of beamforming at the IRS requires channel state information (CSI) for the each reflected path. This is particularly challenging when there are multiple IRSs that need to be identified and channels estimated. Moreover, the pilot-related overhead becomes significant due to the massive number of elements on the IRS [2].

In order to overcome the problems, we propose to exploit an IRS in such a way that it acts as a *frequency mixer* with a given frequency. We are inspired by the time-domain digital-coding metasurface implemented in [3], in which the surface element can generate different reflection amplitudes by a digital controller, which ranges from -1 to 1 to represent the reflectivity changes between total inverse reflection and total reflection. Our architecture relies on sinusoidal adjustment of the reflection amplitude with a certain frequency, uniquely associated with a given surface. Thus, an element of the surface acts as a frequency mixer for the reflected signal. This architecture, which we term *Frequency-Mixing IRS (FMx-IRS)* makes the wireless propagation environment nonlinear and introduces new frequencies, not present in the signal sent from the transmitter. With FMx-IRS, each FM operation at an IRS results in two new frequencies. For example, if a receiver obtains a signal through a direct path and through an FMx-IRS that pulsates with a single frequency, then the received signal has three frequencies: the original one through the direct path and two resulting from the FM operation at the IRS that are symmetric around the original carrier frequency. A similar frequency-mixing approach was used in [4] to compensate for Doppler effects caused by user motion.

This way of introducing non-linearity in the propagation environment opens a plethora of new design opportunities. For example, when arriving at the receiver, the signals coming from the IRS can be uniquely identified by their carrier-frequency shifts. This feature simplifies the channel estimation (CE) in IRS-aided systems, which is challenging when the number of elements is very large. With FMx-IRS, the channels from each IRS can be estimated in parallel, potentially leading to a large decrease in the estimation overhead.

In this paper, we lay the foundation for FMx-IRS communications. While at this point this is a rather speculative architecture, there are works [5, 6] that have investigated the basis for physical implementation of this type of schemes. Our objective is to examine it from a communication-theoretic viewpoint and elaborate the unique way to identify the channel from different propagation paths. We start with the two-path channel model to introduce the basic principles behind FMx-IRS and describe the details of the operation. Then we consider the infinite-path channel model to develop guidelines for choosing operating frequency at the surface. We illustrate that channels from different frequency bands can be estimated in parallel and derive the upper bound of the achievable rate that can perfectly predict the system performance.

II. Basic Principles of FMx-IRS Operation

We start with an intuitive example, where a single-antenna user communicates with a single-antenna BS assisted by one element IRS. We adopt a continuous-time model throughout the paper where t is the time variable. Furthermore, we consider continuous-time convolution and Fourier transforms. We consider a single IRS that is equipped with a single frequency reconfigurable module (FRM). The phase manipulation at the FRM is time-variant with a certain frequency f_r. The model can be generalized to multiple IRS, each with multiple FRMs.

A. FRM-Based Operation

Let us assume that the user transmits a narrowband signal. We assume the FRM in the IRS is able to change the amplitude and phase of the incoming narrowband signal according to a time-varying cosine function $\phi(t)$ with frequency f_r:

$$\phi(t) = \cos(2\pi f_r t). \tag{1}$$

J. Yuan, E. D. Carvalho, R. J. Williams and P. Popovski are with the Department of Electronic Systems, Aalborg University, 9220 Aalborg, Denmark (e-mail: {jyu, edc, rjw, petarp}@es.aau.dk).

E. Björnson is with Linköping University, 58183 Linköping, and also with KTH, 16440 Kista, Sweden (e-mail: {emilbjo}@kth.se).

This work has been partially supported by EU H2020 RISE-6G project and the Danish Council for Independent Research DFF-701700271. E. Björnson was supported by the Grant 2019-05068 from the Swedish Research Council.

This article has been accepted for publication in a future issue of this journal, but has not been fully edited. Content may change prior to final publication. Citation information: DOI 10.1109/LWC.2021.3077085, IEEE Wireless Communications Letters

With a baseband signal $x = |x|\, e^{j\theta}$ with phase θ, the radio frequency signal transmitted over the air becomes

$$x_{\mathrm{R}}(t) = \Re\left\{ x e^{j2\pi f_c t} \right\} = |x| \cos\left(2\pi f_c t + \theta\right), \tag{2}$$

where f_c is the carrier frequency. The channel from the user to the surface is modeled as a single-path frequency-flat channel with impulse response $h(t) = |h|\, \delta\left(t - \tau_h\right)$ ($\delta(\cdot)$ is Dirac delta function), which remains constant during a symbol duration. The pathloss is $|h|$ and the time delay is τ_h. The signal received at the surface is the convolution of the input signal with the channel impulse response, such that IRS receives:

$$\begin{aligned} s(t) &= \textstyle\int_{-\infty}^{\infty} x_{\mathrm{R}}(t-\tau)\, h(\tau)\, d\tau \\ &= |h|\, |x| \cos\left(2\pi f_c \left(t - \tau_h\right) + \theta\right). \end{aligned} \tag{3}$$

With the FM operation, the signal reflected by the FRM then consists of two component

$$\begin{aligned} r(t) &= s(t)\phi(t) \overset{(a)}{=} r_+(t) + r_-(t) \\ &= \tfrac{1}{2}|h|\,|x| \cos\left(2\pi\left(f_c + f_r\right)t - 2\pi f_c \tau_h + \theta\right) \\ &\quad + \tfrac{1}{2}|h|\,|x| \cos\left(2\pi\left(f_c - f_r\right)t - 2\pi f_c \tau_h + \theta\right). \end{aligned} \tag{4}$$

where (a) is obtained using basic trigonometry. Note that the signal reflected from the IRS appears now at two different carrier frequencies: $f_c + f_r$ and $f_c - f_r$.

We now study the link from the FMx-IRS to the BS, which we also assume is a single-path frequency-flat channel. Hence, the impulse response can be expressed as $g(t) = |g|\delta\left(t - \tau_g\right)$, where g and τ_g represent the pathloss and the time delay. After convolution with the channel $g(t)$, we obtain

$$w(t) = |g|\, r_+\left(t - \tau_g\right) + |g|\, r_-\left(t - \tau_g\right). \tag{5}$$

We will now take the direct path between the user and BS into account, which has impulse response $h_{\mathrm{d}}(t) = |h_{\mathrm{d}}|\delta(t - \tau_{\mathrm{d}})$ with $|h_{\mathrm{d}}|$ being the pathloss and τ_{d} the time delay. The received signal at the BS is then given as

$$y(t) = |h_{\mathrm{d}}||x| \cos(2\pi f_c t - 2\pi f_c \tau_{\mathrm{d}} + \theta) + w(t). \tag{6}$$

At the BS, the signal is demodulated to baseband and low-pass filtered. With the in-phase and quadrature demodulation at f_c, the signal has the following form:

$$y_{\mathrm{de}}(t) = y(t) \cos\left(2\pi f_c t\right) + j y(t) \sin\left(2\pi f_c t\right). \tag{7}$$

After a low-pass filter, the output of (7) is

$$\begin{aligned} y_{\mathrm{de}}^{\mathrm{lp}}(t) &= |h_{\mathrm{d}}|\,|x|\, e^{j(-2\pi f_c \tau_{\mathrm{d}} + \theta)} \\ &\quad + \tfrac{1}{2}|h|\,|x|\,|g|\, e^{j(2\pi f_r t - 2\pi(f_c + f_r)\tau_g - 2\pi f_c \tau_h + \theta)} \\ &\quad + \tfrac{1}{2}|h|\,|x|\,|g| e^{j(-2\pi f_r t - 2\pi(f_c - f_r)\tau_g - 2\pi f_c \tau_h + \theta)}. \end{aligned} \tag{8}$$

It is represented in the frequency domain by

$$\begin{aligned} Y(f) &= h_{\mathrm{d}} x \delta(f) \\ &\quad + \tfrac{1}{2} h x g_+ \delta\left(f - f_r\right) + \tfrac{1}{2} h x g_- \delta\left(f + f_r\right), \end{aligned} \tag{9}$$

where $h_{\mathrm{d}} = |h_{\mathrm{d}}| e^{-j2\pi f_c \tau_{\mathrm{d}}}$, $h = |h| e^{-j2\pi f_c \tau_h}$, and $g_\pm = |g|\, e^{-j2\pi(f_c \pm f_r)\tau_g}$. Note that with the FM operation for the RF signal, the phase shift at the baseband signal is then fixed as $\pm 2\pi f_r \tau$ for the signals at f_r and $-f_r$. The separability of the components in (9) enables identification of the signals from the direct and the paths reflected from the IRS:

$$\begin{cases} y_{\mathrm{d}} = h_{\mathrm{d}} x \delta(f), \\ y_+ = z_+ x \delta(f - f_r), \\ y_- = z_- x \delta(f + f_r), \end{cases} \tag{10}$$

where $z_\pm = \frac{1}{2} h g_\pm$. We denote this as a *decoupling feature*.

This feature of an FMx-IRS system is not only appearing in the two-path scenario, but also exist in scattering environments since the frequency of every path reflected by the FRM is shifted by $\pm f_r$. Therefore, we can always observe two components at new frequencies.[1] However, in a rich scattering environment, reflected paths from FMx-IRS may have some new features which are analyzed in Section II-B.

B. Correlation Analysis

We now consider a more general propagation environment with rich scattering, where the channel of each link consists of a large number of paths. We first elaborate that the small-scale fading of all channels asymptotically follow a complex Gaussian distribution and then illustrate the correlation between the two reflected channels at the new frequencies.

Assume that the normalized impulse responses of the channel from the user to BS $h_{\mathrm{d}}(t)$, the user to the surface $h(t)$ and the surface to the BS $g(t)$ can be decomposed as the sum of I, N, and L propagation paths, respectively:

$$h(t) = \sum\nolimits_{i=1}^{I} |h_i| \delta\left(t - \tau_{h,i}\right), \tag{11}$$

$$h_{\mathrm{d}}(t) = \sum\nolimits_{n=1}^{N} |h_{\mathrm{d},n}| \delta\left(t - \tau_{h_{\mathrm{d}},n}\right), \tag{12}$$

$$g(t) = \sum\nolimits_{l=1}^{L} |g_l| \delta\left(t - \tau_{g,l}\right), \tag{13}$$

where h_i, $h_{\mathrm{d},n}$, and g_l represent the amplitude, and $\tau_{h,i}$, $\tau_{h_{\mathrm{d}},n}$ and $\tau_{g,l}$ represent the corresponding delays. Since the transmission of a narrowband signal is considered in the paper, the symbol interval is assumed to be much larger than the maximum delay of all paths and channels are assumed to be constant during a symbol interval.

Applying the same derivations in Section II-A, the baseband equivalent channels in (9) can then be expressed as $h = \sum_{i=1}^{I} h_i$, $h_{\mathrm{d}} = \sum_{n=1}^{N} h_{\mathrm{d},n}$, and

$$g_\pm = \sum\nolimits_{l=1}^{L} g_{\pm,l} \tag{14}$$

in the frequency domain, where $h_i = |h_i|\, e^{-j2\pi f_c \tau_{h,i}}$, $h_{\mathrm{d},n} = |h_{\mathrm{d},n}|\, e^{-j2\pi f_c \tau_{h_{\mathrm{d}},n}}$, and $g_{\pm,l} = |g_l|\, e^{-j2\pi(f_c \pm f_r)\tau_{g,l}}$.

Lemma 1: Suppose τ follows a uniform distribution with probability density function (PDF) $f_\tau(\tau) = \frac{1}{D}$ ranging from 0 to D. For any scalar a, we have following expectations:

$$\mathsf{E}_\tau\left\{\cos\left(2\pi a \tau\right)\right\} = \tfrac{\sin(2\pi a D)}{2\pi a D}, \tag{15}$$

$$\mathsf{E}_\tau\left\{\sin\left(2\pi a \tau\right)\right\} = \tfrac{1 - \cos(2\pi a D)}{2\pi a D}, \tag{16}$$

$$\mathsf{E}_\tau\left\{\cos\left(2\pi a \tau\right)^2\right\} = \tfrac{1}{2} + \tfrac{\sin(4\pi a D)}{8\pi a D}, \tag{17}$$

$$\mathsf{E}_\tau\left\{\sin\left(2\pi a \tau\right)^2\right\} = \tfrac{1}{2} - \tfrac{\sin(4\pi a D)}{8\pi a D}. \tag{18}$$

[1]Differently from the standard two-path interference model, with FMx-IRS, the direct and reflected signals from the surface are separated at different frequencies and the pathloss does not fluctuate according to the phase difference of the two signals. Nevertheless, as the received signal has a larger bandwidth compared to the original one, multiuser interference management will face new challenges.

This article has been accepted for publication in a future issue of this journal, but has not been fully edited. Content may change prior to final publication. Citation information: DOI 10.1109/LWC.2021.3077085, IEEE Wireless Communications Letters

From (14), we can rewrite $g_{\pm}$ as

$$g_{\pm} = \sum\nolimits_{l=1}^{L} |g_l| \cos\left(2\pi \left(f_c \pm f_r\right) \tau_{g,l}\right) - j \sum\nolimits_{l=1}^{L} |g_l| \sin\left(2\pi \left(f_c \pm f_r\right) \tau_{g,l}\right). \quad (19)$$

Let $\tau_{\max}$ be the maximum delay among all paths. It is reasonable to assume that the delays of L paths are uniformly distributed in the range $[0, \tau_{\max}]$. Therefore, according to Lemma 1, since $f_c \pm f_r \gg (2\pi\tau_{\max})^{-1}$, the means of the real part and the imaginary part of $g_{\pm,l}$ are approximately equal to 0, and their variance approximately equal $1/2$. Along with the fact that $\mathsf{E}\{|g_l|^2\} = 1/L$, and according to the Central Limit Theorem, when L goes to infinity, the distribution of $g_{\pm}$ tends toward a complex normal distribution, i.e., $g_{\pm} \sim \mathcal{CN}(0,1)$. Similarly, we can obtain that $h \sim \mathcal{CN}(0,1)$ and $h_{\mathrm{d}} \sim \mathcal{CN}(0,1)$ using the same method.

The channel h and h_{d} are mutually independent, and are independent with $g_{\pm}$ by nature due to the different propagation environments. However, since g_+ and g_- share the same amplitude and the delay, it is necessary to evaluate the correlation between the two reflected channels.

Proposition 1: The correlation $\rho(f_r) = \left|\mathsf{E}_{g_l,\tau_{g,l}}\left\{g_+ g_-^H\right\}\right|$ with respect to the frequency shift f_r is given as

$$\rho(f_r) = \frac{\sqrt{2-2\cos(4\pi f_r \tau_{\max})}}{4\pi f_r \tau_{\max}}. \quad (20)$$

Proof: Noting that the L paths in $g_{\pm}$ are mutually independent as they involve independent random variables, the correlation $\rho(f_r)$ is

$$\rho(f_r) = \left|\mathsf{E}_{g_l,\tau_{g,l}}\left\{\left(\sum\nolimits_{l=1}^{L} g_{+,l}\right)\left(\sum\nolimits_{l'=1}^{L} g_{-,l'}^H\right)\right\}\right| = \left|\mathsf{E}_{g_l,\tau_{g,l}}\left\{\sum\nolimits_{l=1}^{L} g_{+,l} g_{-,l}^H\right\}\right|. \quad (21)$$

Hence, by observing that g_l and $\tau_{g,l}$ are mutually independent with $\mathsf{E}\{|g_l|^2\} = 1/L$, we can compute (21) as

$$\rho(f_r) = L\mathsf{E}\{|g_l|^2\}\left|\mathsf{E}_{\tau_{g,l}}\left\{e^{-j4\pi f_r \tau_{g,l}}\right\}\right| \overset{(b)}{=} \sqrt{\left(\frac{\sin(4\pi f_r \tau_{\max})}{4\pi f_r \tau_{\max}}\right)^2 + \left(\frac{1-\cos(4\pi f_r \tau_{\max})}{4\pi f_r \tau_{\max}}\right)^2} = \frac{\sqrt{2-2\cos(4\pi f_r \tau_{\max})}}{4\pi f_r \tau_{\max}}, \quad (22)$$

where (b) is obtained using (15) and (16). ■

Proposition 1 provides a guideline for the selection of f_r. Suppose we select $f_r = i\Delta f$ where $\Delta f = 1/(2\tau_{\max})$ and i is a positive integer. We then obtain two uncorrelated channels g_+ and g_- at new frequencies.

C. Decoupling Feature

As illustrated in Fig. 1(b), the frequency response of the received signal consists of three components with two of them around $f_c \pm f_r$. Since the channels are decoupled in the frequency domain, one pilot can estimate all three channels, which we call the channel decoupling feature. This is significantly different from a conventional IRS system, where one element generates one channel, and the reflective channel is coupled with the channel from the direct path at the receiver. To separate the channel of each link, it is required to send two pilot symbols [7]. The decoupling feature is particularly important since, in conventional IRS systems, the pilot overhead required for estimating each link grows linearly with the number of the elements on the surface, which results in a huge degradation of achievable rate under user mobility. However, in an FMx-IRS aided system, each of the FRMs can be associated to a unique frequency, and all the channels reflected by the surface are separable in the frequency domain, thereby sparing the use of pilot sequences. Moreover, although FMx-IRS takes up wider bandwidth as a conventional wideband system does, it shows an essential difference shown in Fig. 1(c). In a conventional wideband system, the power of pilot and data are allocated across the bandwidth B, whereas in an FMx-IRS-aided system, the transmission power is concentrated in a narrow band, thereby observing a much higher SNR at the receiver side.

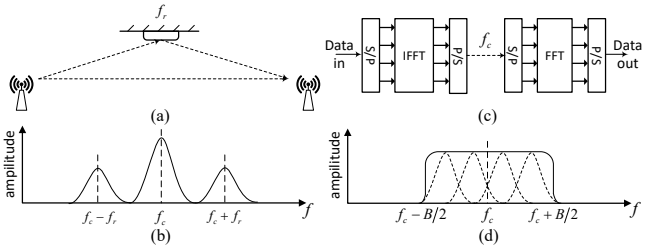

Fig. 1. A simple example of an FMx-IRS-aided system is shown in (a), where a single-antenna transmitter communicates with a single-antenna receiver aided by an FRM operating on frequency f_r; (b) shows the corresponding frequency response of the received signal; (c) give an example of a wideband system with carrier at f_c and bandwidth B, and (d) shows the corresponding frequency response.

III. General System Model

We will now consider a general model in uplink direction where one BS with M antennas serves one single-antenna user aided by one FMx-IRS. We assume that user is randomly located in area while the BS and the surface have fixed positions. The surface is divided into an array of $V \times S$ FRMs, and the (v,s)th FRM carries out a frequency modulation operation at frequency $f_{v,s}$.[2] We assume the frequency spacing between two adjacent frequency shifts is f_n, and $f_{v,s} = ((v-1)S+s)f_n$. Therefore, a single narrowband signal from the transmitter will result in a set of $2SV+1$ received narrowband signals at the receiver, and from those signals we can uniquely estimate the channel response from each FRM.

In this section, all the quantities are in the frequency domain, so that we omit the frequency variable f for simplicity. We denote by $\mathbf{h}_{\mathrm{d}} \in \mathbb{C}^{M\times 1}$ and $h_{v,s} \in \mathbb{C}$ the direct channel from user to the BS and the channel from user to the (v,s)th FRM of the surface, respectively. Regarding the paths from the surface to the BS, each FMx-IRS creates two channels at two different frequency bands. We denote by $\mathbf{g}_{+,v,s} \in \mathbb{C}^{M\times 1}$ and $\mathbf{g}_{-,v,s} \in \mathbb{C}^{M\times 1}$ the channels from the (v,s)th FRM to the BS at frequency $f_c \pm f_{v,s}$.

We assume that $|x| = 1$ is a complex signal variable that can represent either a pilot or data symbol. The frequency-domain received signal $\mathbf{y} \in \mathbb{C}^{(2VS+1)M\times 1}$ is then written as

$$\mathbf{y} = \sqrt{p}\mathbf{h}_{\mathrm{all}} x + \mathbf{n}, \quad (23)$$

[2]In practice, FRMs can be split into a small number of subarrays with each subarray associated with one frequency, thereby reducing the hardware cost and simplifying the signal composition.

where p is the normalized power of each symbol,

$$\mathbf{y} = \left[\mathbf{y}_{\mathrm{d}}^T, \mathbf{y}_{+,1,1}^T, \mathbf{y}_{-,1,1}^T, \cdots, \mathbf{y}_{+,V,S}^T, \mathbf{y}_{-,V,S}^T\right]^T, \quad (24)$$

$$\mathbf{h}_{\text{all}} = \left[\mathbf{h}_{\mathrm{d}}^T, \mathbf{z}_{+,1,1}^T, \mathbf{z}_{-,1,1}^T, \cdots, \mathbf{z}_{+,V,S}^T, \mathbf{z}_{-,V,S}^T\right]^T \quad (25)$$

with $\mathbf{z}_{\pm,v,s} = \frac{1}{2} h_{v,s} \mathbf{g}_{\pm,v,s}$ representing the cascaded channel from the user to the (v,s)th FRM at surface to the BS. $\mathbf{n} \in \mathbb{C}^{(2VS+1)M\times 1}$ is AWGN with i.i.d. $\mathcal{CN}(0,1)$ elements.

IV. Channel Estimation and Downlink Precoder Design In FMx-IRS-Aided Systems

In this section, we illustrate that conventional channel estimation algorithms can be applied to different propagation environments and derive the achievable rates for the FMx-IRS-assisted systems.

A. Channel Model

1) Two-Path model: For this model, the pathloss and the delay depend on the distance of the propagation path. We assume that the 3D coordinate of the user, the first BS antenna, and the $(1,1)$th FRM at the surface are $\mathbf{o}_{\mathrm{u}} = (b_{\mathrm{u}}, e_{\mathrm{u}}, u_{\mathrm{u}})$, $\mathbf{o}_{\mathrm{b},1} = (b_{\mathrm{b}}, e_{\mathrm{b}}, u_{\mathrm{b}})$ and $\mathbf{o}_{\mathrm{s},1,1} = (b_{\mathrm{s}}, e_{\mathrm{s}}, u_{\mathrm{s}})$, respectively. Therefore, the coordinates of the mth BS antenna and the (v,s)th FRM at the surface are given by $\mathbf{o}_{\mathrm{b},m} = (b_{\mathrm{b}} + (m-1)d_{\mathrm{b}}, e_{\mathrm{b}}, u_{\mathrm{b}})$ and $\mathbf{o}_{\mathrm{s},v,s} = (b_{\mathrm{s}}, e_{\mathrm{s}} + (v-1)d_{\mathrm{s}}, u_{\mathrm{s}} + (s-1)d_{\mathrm{s}})$ with d_{b} and d_{s} being the antenna spacing at the BS and the FRM spacing at the surface.

Using these coordinates, the channel components of the user-surface link, user-BS link and surface-BS link can be modelled as $h_{v,s} = |h_{v,s}|\, e^{-j\kappa\|\mathbf{o}_{\mathrm{u}} - \mathbf{o}_{\mathrm{s},v,s}\|}$, $h_{\mathrm{d},m} = |h_{\mathrm{d},m}|\, e^{-j\kappa\|\mathbf{o}_{\mathrm{u}} - \mathbf{o}_{\mathrm{b},m}\|}$, and $g_{\pm,v,s,m} = |g_{v,s,m}|\, e^{-j\kappa_{\pm,v,s}\|\mathbf{o}_{\mathrm{b},m} - \mathbf{o}_{\mathrm{s},v,s}\|}$, where $|h_{v,s}| = (\|\mathbf{o}_{\mathrm{u}} - \mathbf{o}_{\mathrm{s},v,s}\|/d_0)^{-\alpha}$, $|h_{\mathrm{d},m}| = (\|\mathbf{o}_{\mathrm{u}} - \mathbf{o}_{\mathrm{b},m}\|/d_0)^{-\alpha}$, and $|g_{v,s,m}| = (\|\mathbf{o}_{\mathrm{b},m} - \mathbf{o}_{\mathrm{s},v,s}\|/d_0)^{-\alpha}$ with d_0 representing the reference distance according Friis transmission formula; $\kappa = \frac{2\pi f_c}{c}$ and $\kappa_{\pm,v,s} = \frac{2\pi(f_c \pm f_{v,s})}{c}$ with c being the light speed; α represents the pathloss exponent with typical value $\alpha = 2$ representing the LoS scenario. Therefore, the cascaded channel is given as

$$z_{\pm,v,s,m} = |z_{v,s,m}| e^{-j(\kappa\|\mathbf{o}_{\mathrm{u}} - \mathbf{o}_{\mathrm{s},v,s}\| + \kappa_{\pm,v,s}\|\mathbf{o}_{\mathrm{b},m} - \mathbf{o}_{\mathrm{s},v,s}\|)}, \quad (26)$$

where $|z_{v,s,m}| = |\frac{1}{2} h_{v,s} g_{v,s,m}|$. Note that the channel of the surface-BS link is deterministic due to the fixed position of the surface and the BS.

2) Infinite-Path Model: Omitting the slight difference in pathloss between adjacent antennas, we denote by β_{d}, β_{ur}, and β_{rb} the pathloss of user-BS link, user-IRS link and IRS-BS link, respectively. We obtain $h_{\mathrm{d},m} \sim \mathcal{CN}(0, \beta_{\mathrm{d}})$ and $h_{v,s} \sim \mathcal{CN}(0, \beta_{\mathrm{ur}})$ when the number of paths grow large. Regarding the channels from the surface to the BS, instead of simply assuming they are complex Gaussian value, it is required to model each of them as the sum of L ($L \to \infty$) paths:

$$g_{\pm,v,s,m} = \sum\nolimits_{l=1}^{L} g_{\pm,v,s,m,l}, \quad (27)$$

where $g_{\pm,v,s,m,l} = |g_{v,s,m,l}|\, e^{-j2\pi(f_c \pm f_{v,s})\tau_{v,s,m,l}}$, since $g_{+,v,s,m}$ and $g_{-,v,s,m}$ are not mutually independent. Moreover, we model the amplitude and the delay of the lth path randomly as $\mathsf{E}\{|g_{v,s,m,l}|^2\} = \beta_{\mathrm{rb}}/L$ and $\tau_{v,s,m,l}$ uniformly distributed in $[0, \tau_{\max}]$. In this manner, the small scale fading of $g_{+,v,s,m}$ and $g_{-,v,s,m}$ follow a complex Gaussian distribution with the correlation being $\beta_{\mathrm{rb}}\rho(f_{v,s})$. Therefore, the cascaded channel $z_{\pm,v,s,m} = \frac{1}{2} h_{v,s} g_{\pm,v,s,m}$ is then the product of two complex Gaussian variables, and follows a complex product-normal distribution [8], which is symmetric around the origin with the variance being $\beta_{\mathrm{ur}}\beta_{\mathrm{rb}}/4$.

B. Channel Estimation

Since $\mathbf{h}_{\mathrm{d}}$, $\mathbf{z}_{\pm,s,v}$ are decoupled in the frequency domain, their estimation can be performed in parallel. We discuss the CE methods separately for channel statistics are known or unknown.

1) Least Squares estimator: When channel statistics are unknown at BS, the conventional least squares estimator can be applied. We obtain the channel estimates as

$$\hat{\mathbf{h}}_{\text{all}} = \tfrac{1}{\sqrt{p}} x^* \mathbf{y}, \quad (28)$$

where x^* represents the conjugate transpose of x. The estimation error $\tilde{\mathbf{h}}_{\text{all}} = \hat{\mathbf{h}}_{\text{all}} - \mathbf{h}_{\text{all}}$ has i.i.d. elements with $\mathsf{var}\{\tilde{h}_{\mathrm{d},m}\} = |h_{\mathrm{d},m}|^2/p$, and $\mathsf{var}\{\tilde{z}_{\pm,v,s,m}\} = |z_{v,s,m}|^2/p$.

2) Minimum mean square error (MMSE): With channel statistics known at the receiver, We can apply MMSE approach to estimate $\mathbf{h}_{\text{all}}$. Noting that the estimation of $\mathbf{h}_{\mathrm{d}}$, $\mathbf{z}_{\pm,v,s}$ are decoupled. We obtain the MMSE estimator as [9]:

$$\hat{\mathbf{h}}_{\mathrm{d}} = \tfrac{1}{\sqrt{p}} \mathbf{y}_{\mathrm{d}} x^* (1 + 1/(p\beta_{\mathrm{d}}))^{-1}, \quad (29)$$

$$\hat{\mathbf{z}}_{\pm,v,s} = \tfrac{1}{\sqrt{p}} \mathbf{y}_{\pm,v,s} x^* (4 + 1/(p\beta_{\mathrm{ur}}\beta_{\mathrm{rb}}))^{-1} \quad (30)$$

by realizing that the covariance matrix of LoS channel and the cascaded channel are $\beta_{\mathrm{d}}\mathbf{I}_M$ and $\frac{1}{4}\beta_{\mathrm{ur}}\beta_{\mathrm{rb}}\mathbf{I}_M$, respectively. Let $\tilde{\mathbf{h}}_{\mathrm{d}} = \hat{\mathbf{h}}_{\mathrm{d}} - \mathbf{h}_{\mathrm{d}}$ and $\tilde{\mathbf{z}}_{\pm,v,s} = \hat{\mathbf{z}}_{\pm,v,s} - \mathbf{z}_{\pm,v,s}$ being the channel estimation error vector for the direct path and reflected paths at $f_c \pm f_s$, respectively. The variance of elements of estimation error for direct path and reflect path are equal to $\mathsf{var}\{\tilde{h}_{\mathrm{d},m}\} = \frac{\beta_{\mathrm{d}}}{1+p}$, and $\mathsf{var}\{\tilde{z}_{\pm,v,s,m}\} = \frac{\beta_{\mathrm{ur}}\beta_{\mathrm{rb}}}{1+(1/4)p}$, respectively [9]. Equations (28), (29) and (30) indicate that the pilot-based channel estimation scheme is feasible for estimating the cascaded channel for both two-path model and multipath model without requiring extra pilot overhead.

C. Rate Analysis for Infinite-path Model

Assuming that perfect CSI is available at the BS, the achievable rate can be written in the following form:

$$R_{\mathrm{p}} = \mathsf{E}_{\mathbf{h}_{\text{all}}}\left[\log_2(1 + p\mathbf{h}_{\text{all}}^H \mathbf{h}_{\text{all}})\right]. \quad (31)$$

An analytical evaluation of (31) is complicated due to the different distribution of the direct channel and cascaded channel. However, using Jensens inequality, we can compute and upper bound on the achievable rate in closed form:

$$R_{\mathrm{p}} \leqslant \log_2\left(1 + p\mathsf{E}_{\mathbf{h}_{\text{all}}}\left[\mathbf{h}_{\text{all}}^H \mathbf{h}_{\text{all}}\right]\right). \quad (32)$$

Based on the statistic properties given in Section IV-B, it follows that

$$\mathsf{E}_{\mathbf{h}_{\text{all}}}\left[\mathbf{h}_{\text{all}}^H \mathbf{h}_{\text{all}}\right] = M\beta_{\mathrm{d}} + \beta_{\mathrm{ur}}\beta_{\mathrm{rb}}\frac{MSV}{2}. \quad (33)$$

Proposition 2: With perfect CSI, the achievable rate for the FMx-IRS-aided system is upper bounded by

$$R_{\mathrm{p}} \leqslant \log_2\left(1 + pM\left(\beta_{\mathrm{d}} + \beta_{\mathrm{ur}}\beta_{\mathrm{rb}}\frac{SV}{2}\right)\right). \quad (34)$$

This article has been accepted for publication in a future issue of this journal, but has not been fully edited. Content may change prior to final publication. Citation information: DOI 10.1109/LWC.2021.3077085, IEEE Wireless Communications Letters

The result indicates that the capacity grows linearly with the number of FRMs on the surface.

V. Numerical Results

In the simulation, we set the coordinates of the first BS antenna and the $(1,1)$th FRM at the surface at $\mathbf{o}_{\mathrm{b},1} = (30,30,10)\,\mathrm{m}$ and $\mathbf{o}_{\mathrm{s},1,1} = (0,0,4)\,\mathrm{m}$, respectively. The antenna spacing and FRM spacing are set as $d_{\mathrm{b}} = 0.1\,\mathrm{m}$, $d_{\mathrm{s}} = 0.1\,\mathrm{m}$, while the reference distance is set as $d_0 = 50\,\mathrm{m}$. Moreover, the carrier frequency and the maximum delay are set as $f_c = 2\,\mathrm{GHz}$ and $\tau_{\max} = 10^{-5}\,\mathrm{s}$, respectively.

Fig. 2 compares the channel gain of the classical two-path model and the two-path model in which one of the paths goes through an FMx-RIS. The fluctuations in the classical two-path model are due to the superposition of the two rays with different phases. FMx-RIS decouples the two paths in frequency and avoids this superposition, which stabilizes the channel gain of the received signal as a function of distance, at the expense of a larger occupied bandwidth.

Fig. 3 exhibits the normalized MSE (NMSE) of channel estimation under different propagation environment. We observe that the estimation performance of the direct path outperforms that of the reflected path at low-SNR. This is due to the fact that the frequency-mixing operation splits the power, and the effect of noise on channel estimation at low SNRs is much higher than that in a high SNR regime.

In Fig. 4(a), we illustrate the condition number of matrix $\mathbf{F} = \mathsf{E}\{\mathbf{h}_{\mathrm{all}}\mathbf{h}_{\mathrm{all}}^H\}$ to show the channel diversity gain. We observe that when i is an integer, the condition number $\eta(\mathbf{F})$ is $0\,\mathrm{dB}$, indicating that $\mathbf{F}$ is an identity matrix as expected. Moreover, when the frequency spacing is small, the more FRMs the surface contain, the closer $\mathbf{F}$ to being singular, meaning that less number of streams can be transmitted. Fig. 4(b) compares the tightness of the analytical rate upper bound compare with the real capacity. We also include the performance of the conventional MIMO as the benchmark. It can be observed that the upper bound converge to the real achievable rate really tight, indicating that analytical result can perfectly predict the rate performance. Moreover, we can obtain rate gain compared with conventional MIMO which is intuitive due to the extra contribution from the reflected paths.

VI. Conclusion

In the paper, we proposed a novel FMx-IRS-aided system, where the IRS consists of several number modules that are capable of manipulating the frequencies of the incident signals. We first demonstrated the basic principles of the FMx-IRS architecture and illustrated its advantages in terms of channel decoupling. Then, we provided guidelines for choosing the operating frequencies for the infinite-path channel model. The channel estimation is investigated for the different propagation environments, and the upper bound of the achievable rate is derived for the infinite-path channel model. The numerical results indicate the tightness of rate bound, and with the appropriate operating frequencies, FMx-IRS generates a nearly i.i.d. propagation environment. Clearly, the concept of FMx-IRS challenges the present notion of frequency occupancy determined by the transmitter and can have consequences for spectrum allocation and interference management.

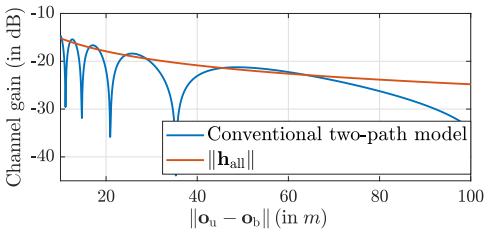

Fig. 2. Pathloss v.s. distance between user and BS under two-path model. The result is shown for $V, S, M = 1$ and $f_n = 0.1\Delta f$.

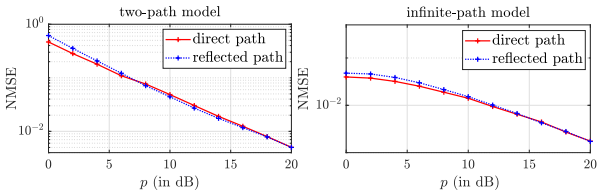

Fig. 3. Channel NMSE v.s. the transmit power for different channel model. The results are shown for $V, S = 2$, $\mathbf{o}_{\mathrm{u}} = (-50,30,1)\,\mathrm{m}$, and $\beta_{(\cdot)} = (d_{(\cdot)}/d_0)^{-\alpha}$, where $d_{(\cdot)}$ represents the distance of transmission link.

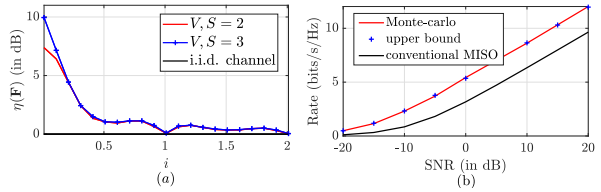

Fig. 4. Impact of correlation among reflected paths under infinite-path model, in which (a) shows the conditioning number of $\mathbf{F}$ w.r.t $i = f_n/\Delta f$; (b) compares the capacity upper bounds with real capacity where $f_n = \Delta f$, $V = S = 2$, and $M = 8$.

References

[1] M. D. Renzo *et al.*, "Smart radio environments empowered by reconfigurable intelligent surfaces: How it works, state of research, and road ahead," *IEEE J. Sel. Areas Commun.*, vol. 38, no. 11, pp. 2450–2525, 2020.

[2] E. Björnson, Ö. Özdogan, and E. G. Larsson, "Reconfigurable intelligent surfaces: Three myths and two critical questions," *IEEE Com. Mag.*, no. 12, pp. 90–96, 2020.

[3] J. Zhao *et al*, "Programmable time-domain digital-coding metasurface for non-linear harmonic manipulation and new wireless communication systems," *National Science Review*, vol. 6, no. 2, pp. 231–238, Nov. 2018.

[4] Z. Huang, B. Zheng, and R. Zhang, "Transforming fading channel from fast to slow: IRS-assisted high-mobility communication," 2020. [Online]. Available: https://arxiv.org/abs/2011.03147

[5] D. Ramaccia, D. L. Sounas, A. Al, A. Toscano, and F. Bilotti, "Phase-induced frequency conversion and doppler effect with time-modulated metasurfaces," *IEEE Transactions on Antennas and Propagation*, vol. 68, no. 3, pp. 1607–1617, 2020.

[6] L. Zhang *et al*, "Space-time-coding digital metasurfaces," *Nat. Commun*, vol. 9, pp. 1–11, Oct. 2018.

[7] T. L. Jensen and E. De Carvalho, "An optimal channel estimation scheme for intelligent reflecting surfaces based on a minimum variance unbiased estimator," in *Proc. IEEE ICASSP*, May 2020, pp. 5000–5004.

[8] S. Nadarajah and T. K. Pogány, "On the distribution of the product of correlated normal random variables," *Comptes Rendus Mathematique*, vol. 354, no. 2, pp. 201–204, 2016.

[9] S. M. Kay, *Fundamentals of Statistical Signal Processing: Estimation Theory*. Englewood Cliff, 1993, vol. 1.